Finite-conical-well model for vertically adsorbed diatomic molecules

Y. T. Shih
Institute of Electro-Optical Engineering, National Chiao Tung University, Hsinchu, Taiwan, Republic of China

D. S. Chuu* and W. N. Mei†
Department of Electrophysics, National Chiao Tung University, Hsinchu, Taiwan, Republic of China
(Received 19 October 1994; revised manuscript received 26 January 1995)

We present studies of the rotational spectra of a diatomic molecule adsorbed vertically on a solid surface. The hindrance configuration was modeled as a rigid rotor whose spatial motion was confined by a finite conical well. The eigenfunctions can be expressed analytically in terms of the hypergeometric functions, and eigenvalues were solved numerically. We found that the rotational energy levels and the confinement probabilities exhibit oscillatory behaviors when plotted as functions of the hindrance angle. The solutions were used to calculate the rotational-state distribution of the suddenly unhindered rotors and general features which agree with the previous experimental findings were obtained.

I. INTRODUCTION

Rotational motion of an adsorbed molecule which depends heavily on its interaction with the substrate is definitely different from that of the free space rotor. Therefore thorough study of the rotational spectra and eigenstates is crucial to the understanding of the dynamics of adsorption and desorption. Recently, the rotational motion of the molecule which interacts with a solid surface has attracted increasing interest. Many experimental studies have been carried out to measure the rotational-state distributions of diatomic molecules scattered,[1–5] thermally desorbed,[6–8] and electron- or photon-stimulatedly desorbed[9–13] from solid surfaces. Kleyn *et al.*[2] measured the rotational-state distributions of NO molecules inelastically scattered from a Ag(111) surface for various incident angles and normal kinetic energies. The distributions they measured could be divided into two portions: a low-rotational-state portion, which was described by a Boltzmann distribution with rotational temperature independent of surface temperature, and a high-rotational-state portion, which showed a broad structure and was interpreted as the result of a rotational rainbow. Cavanagh and King[6] measured rotational-state distributions of NO molecules thermally desorbed from a Ru(001) surface. Their measured distribution was characterized by a Boltzmann distribution with a rotational temperature significantly lower than the surface temperature. Recently Xu *et al.*[13] reported experimental studies of rotational-state distributions of excited CN desorbed from alkali-metal and alkali-metal-halide surfaces by irradiating photons and electrons. Rotational-state distributions were found to exhibit temperature-independent non-Boltzmann features that were uniquely correlated to the particular alkali-metal component of the substrate. From the above stated experimental results, the substrate temperature-independent non-Boltzmann feature is a universal feature of the rotational distribution in diatomic molecule surface scattering and desorption.

For adsorbed molecules, the effect imposed by the substrate surface on the molecules can be regarded as hindering the molecular rotational motion, thus the surface potential is angle-dependent functions. Analytical expressions for the realistic surface potentials are difficult to derive and then usually very complicated to treat. Therefore, in order to acquire deeper theoretical understanding, many simplified models for surface potentials were proposed to simulate the hindered rotational motion. Pacey and Allen[14,15] proposed sinusoidal functions of the polar angle which measured from the surface normal to the molecular axis to model the surface potential. Energy levels and thermodynamic properties of the adsorbed molecule were calculated for these potentials, and comparisons with the experimental data on entropy of adsorption, ortho-para separation, and rates of thermal desorption were discussed. Gadzuk and co-workers[16–19] assumed an angle-dependent hindering potential in the form of the infinite conical well which was the spherical coordinate analog of the Cartesian-coordinate square well and solved the problem analytically. In their model, the rotor was allowed to rotate freely only if the polar angle lies within the conical well. This infinite-conical-well model was used together with a sudden unhindrance approximation to interpret the non-Boltzmann properties of final rotational-state distributions. Krempl[20] used the linear combination of two spherical harmonics to model the angular dependence of the surface potential. Together with the spatial part expressed as an exponential function which depends on the distance between molecule and surface, the rotational cooling effect of desorbed diatomic molecules was reproduced. In addition to the consideration of the polar-angle dependence, the azimuthal-angle dependence of the surface potential has also been considered. The simplest model was to assume the surface potential bears the same symmetry as that

of the solid surface. Both Kronig-Penney type[19,21] and sinusoidal[22] modulated potentials which bear the surface symmetry were used to study the azimuthal motion of the hindered rotor.

The infinite-conical-well model proposed by Gadzuk *et al.* was impressive. It could be treated with simple mathematics while providing a good insight into the interaction between the adsorbed molecule and the surface. However, the hard conical wall precluded completely the probability of a rotor appearing outside the conical well, which may be important for the small conical angle situations, analogous to the narrow finite square well in the Cartesian coordinate. Furthermore, it is very hard to obtain the approximate strength of the interaction between the molecule and the surface by comparing the theoretical result obtained from solving the infinite-conical-well model with the experimental data. Thus it is interesting to investigate the hindered rotational motion with a more realistic, let us say, finite hindering potential. But this is not a straightforward modification, because we cannot prescribe an exponentially decaying solution at the potential barrier region as we usually do in the Cartesian finite potential well problems. Because the total Hamiltonian is rotationally invariant, i.e., solutions have to remain the same after n complete rotations, where n is an integer, one has to study carefully the properties of the solutions in the previously forbidden region, i.e, $\alpha \leq \theta \leq \pi$.

In this paper, we present a simple finite-conical-well model by which the hindered rotational motion of a vertically adsorbed molecule is modeled [see Fig. 1(a)]. In Sec. II, the mathematical techniques used to solve the model exactly are discussed in detail. Results obtained from solving the model analytically were used to illustrate the variations of the eigenstates and energy spectra for different barrier heights and conical angles are presented in Sec. III. By making use of them, we also calculated the rotational-state distributions. Together with experimental information,[1–13] we can extract the interaction strength between the adsorbed molecule and the substrate, and the nature of the dynamics which is responsible for the processes occurring on the surface. In Sec. IV, brief conclusions are given. We plan to discuss the rotational motion of a horizontally adsorbed molecule hindered by a finite-conical-well potential [see Fig. 1(b)] in a future paper.[23]

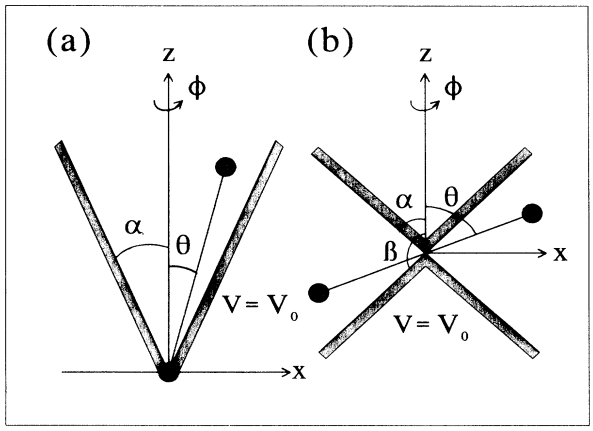

FIG. 1. (a) Schematic of the finite-conical-well hindering potential for vertical adsorption configuration. (b) Schematic of the finite-conical-well hindering potential for horizontal adsorption configuration.

II. THE MODEL

Consider a diatomic molecule vertically adsorbed by a solid surface where the adsorption configuration is shown in Fig. 1(a). The molecular vibrational motion along the molecular axis is neglected by regarding the molecule as a rigid dumbbell. The constraint imposed by the solid surface upon the molecule is assumed to hinder the molecular rotational motion, thus the angular part of the Schrödinger equation for such hindered rotation is given by

$$\left\{\frac{1}{\sin\theta}\frac{\partial}{\partial\theta}\left(\sin\theta\frac{\partial}{\partial\theta}\right)+\frac{1}{\sin^2\theta}\frac{\partial^2}{\partial\phi^2}+\frac{2I}{\hbar^2}\left[E^{\mathrm{rot}}_{\nu,m}-V^{\mathrm{hin}}(\theta,\phi)\right]\right\}\Psi^{\mathrm{rot}}_{\nu,m}(\theta,\phi)=0, \quad (1)$$

where I is the molecular moment of inertia with respect to its center of rotation. The subscripts ν and m contained in the eigenenergy $E^{\mathrm{rot}}_{\nu,m}$ and wave function $\Psi^{\mathrm{rot}}_{\nu,m}$ represent the quantum numbers arising from the dependence of hindering potential V^{hin} upon θ and ϕ.

As proposed by Gadzuk *et al.*, one may assume a ϕ-independent conical well to model the hindering potential, i.e., free rotations of the molecule are allowed provided the polar angle lies within the region $0 \leq \theta < \alpha$. However, in contrast to Gadzuk's hard-wall rotor which appeared only in the region $0 \leq \theta < \alpha$, we used a soft wall with height V_0B in the region $\alpha \leq \theta \leq \pi$ and the hindered rotations are allowed in the region, i.e.,

$$V^{\mathrm{hin}}(\theta,\phi)=\begin{cases}0 & \text{for } 0\leq\theta<\alpha\\ V_0B & \text{for } \alpha\leq\theta\leq\pi,\end{cases} \quad (2)$$

where B is the rotational constant of the molecule: $B = \hbar^2/2I$, and V_0 is a dimensionless potential strength parameter.

For the ϕ-independent hindering potential the total angular part of the wave function can be simply separated as

$$\Psi^{\mathrm{rot}}_{\nu,m}(\theta,\phi)=\Theta_{\nu,m}(\theta)\,\Phi_m(\phi), \quad (3)$$

with

$$\Phi_m(\phi)=\frac{1}{\sqrt{2\pi}}\exp(im\phi), \quad m=0,\pm1,\pm2,\ldots . \quad (4)$$

Here, we express the rotational energy in the form

$$E^{\mathrm{rot}}_{\nu,m}=\nu(\nu+1)B, \quad (5)$$

which makes an obvious connection with the limit of free rotation, and define ν' as

$$\nu'(\nu'+1) = \nu(\nu+1) - V_0, \tag{6}$$

then the θ part of Eq. (1) can be expressed in terms of the auxiliary variable $\xi = \cos\theta$ as

$$\frac{d}{d\xi}\left[\left(1-\xi^2\right)\frac{d\Theta_{\mathrm{I},\nu,m}}{d\xi}\right] + \left[\nu(\nu+1) - \frac{m^2}{1-\xi^2}\right]\Theta_{\mathrm{I},\nu,m} = 0 \text{ for } \cos\alpha < \xi \leq 1 \tag{7a}$$

and

$$\frac{d}{d\xi}\left[\left(1-\xi^2\right)\frac{d\Theta_{\mathrm{II},\nu,m}}{d\xi}\right] + \left[\nu'(\nu'+1) - \frac{m^2}{1-\xi^2}\right]\Theta_{\mathrm{II},\nu,m} = 0 \text{ for } -1 \leq \xi \leq \cos\alpha. \tag{7b}$$

Equations (7a) and (7b) are the associated Legendre equations[24,25] with integer order m; the degrees ν and ν' are, however, not necessarily integers.

Changing variable $\eta = (1-\xi)/2$ and denoting

$$\Theta_{\nu,m}(\xi) = A_{\nu,m}\left(1-\xi^2\right)^{|m|/2} W(\xi), \tag{8}$$

where $A_{\nu,m}$ is the normalization constant, Eqs. (7a) and (7b) can then be reduced to

$$\eta(1-\eta)\frac{d^2W_{\mathrm{I}}}{d\eta^2} + (|m|+1)(1-2\eta)\frac{dW_{\mathrm{I}}}{d\eta} - (|m|-\nu)(|m|+\nu+1)W_{\mathrm{I}} = 0 \text{ for } 0 \leq \eta < (1-\cos\alpha)/2, \tag{9a}$$

and

$$\eta(1-\eta)\frac{d^2W_{\mathrm{II}}}{d\eta^2} + (|m|+1)(1-2\eta)\frac{dW_{\mathrm{II}}}{d\eta} - (|m|-\nu')(|m|+\nu'+1)W_{\mathrm{II}} = 0 \text{ for } (1-\cos\alpha)/2 \leq \eta \leq 1. \tag{9b}$$

Solving Eqs. (9a) and (9b) requires further investigation of the properties of the hypergeometric functions. As we compare them to the standard form[24,25]

$$z(1-z)\frac{d^2W}{dz^2} + [\gamma - (\alpha+\beta+1)z]\frac{dW}{dz} - \alpha\beta W = 0, \tag{10}$$

where we can easily find that, for Eq. (9a),

$$\begin{aligned}\alpha &= |m| - \nu,\\ \beta &= |m| + \nu + 1,\\ \gamma &= |m| + 1,\end{aligned} \tag{11}$$

from comparison. Then the wave function for region $0 \leq \theta < \alpha$ is

$$\Theta_{\mathrm{I},\nu,m}(\xi) = A_{\mathrm{I},\nu,m}\left(1-\xi^2\right)^{|m|/2} \times F\left(|m|-\nu, |m|+\nu+1, |m|+1; \frac{1-\xi}{2}\right), \tag{12}$$

where $F(\alpha,\beta,\gamma;z)$ is the hypergeometric function which is finite when $\xi = 1\,(\theta = 0)$. But the solution diverges when $\xi = -1\,(\theta = \pi)$, unless $|m| - \nu = -n$, where n is zero or a positive integer, then Eq. (12) terminates at finite terms. But this corresponds to the case of a free space rotor. On the other hand, in order to solve Eq. (9b), we have to study the behavior of Eq. (10) at the neighborhood of $z = 1$. It is more convenient to replace z by $1-z$; Eq. (10) then changes into

$$z(1-z)\frac{d^2W}{dz^2} + [(\alpha+\beta-\gamma+1) - (\alpha+\beta+1)z]\frac{dW}{dz} - \alpha\beta W = 0. \tag{13}$$

Making use of Eqs. (11) and (12), the solution can be found as

$$\Theta_{\mathrm{II},\nu,m}(\xi) = A_{\mathrm{II},\nu,m}\left(1-\xi^2\right)^{|m|/2} F\left(|m|-\nu', |m|+\nu'+1, |m|+1; \frac{1+\xi}{2}\right). \tag{14}$$

We can easily see that Eq. (14) is identical to Eq. (12) except for the case that each of them is expressed in terms of different variables. Again, Eq. (14) is finite when $\xi = -1\,(\theta = \pi)$, but diverges at $\xi = 1$ unless we follow the previous scheme by setting $|m| - \nu' = -n$. Now, following the same fashion as in the Cartesian counterpart we have constructed solutions Θ_{I} and Θ_{II} in two different regions; they are both rotational invariant and well behaved around each other's singularity. The wave function can be written as

$$\Theta_{v,m}(\xi) = \begin{cases} A_{\mathrm{I},\nu,m}\left(1-\xi^2\right)^{|m|/2} F\left(|m|-\nu, |m|+\nu+1, |m|+1; \frac{1-\xi}{2}\right) & \text{for } \cos\alpha < \xi \leq 1\\ A_{\mathrm{II},\nu,m}\left(1-\xi^2\right)^{|m|/2} F\left(|m|-\nu', |m|+\nu'+1, |m|+1; \frac{1+\xi}{2}\right) & \text{for } -1 \leq \xi \leq \cos\alpha, \end{cases} \tag{15}$$

which is normalized by the following relation:

$$\int_{-1}^{1} d\xi\, |\Theta_{\nu,m}(\xi)|^2 = 1. \tag{16}$$

In order to determine ν, we have to match the logarithmic derivatives of $\Theta_{\mathrm{I},\nu,m}$ and $\Theta_{\mathrm{II},\nu,m}$ at $\theta=\alpha$. Making use of the differential formula[24]

$$\frac{d}{dz}F(a,b,c;z)=\frac{ab}{c}F(a+1,b+1,c+1;z), \tag{17}$$

we have arrived at the following equation which determines the eigenvalues of the soft-wall hindered rotor:

$$\frac{(|m|-\nu)(|m|+\nu+1)}{(|m|+1)}\frac{F\left(|m|-\nu+1,|m|+\nu+2,|m|+2;\frac{1-\xi}{2}\right)}{F\left(|m|-\nu,|m|+\nu+1,|m|+1;\frac{1-\xi}{2}\right)}\Bigg|_{\xi=\cos\alpha}$$
$$+\frac{(|m|-\nu')(|m|+\nu'+1)}{(|m|+1)}\frac{F\left(|m|-\nu'+1,|m|+\nu'+2,|m|+2;\frac{1+\xi}{2}\right)}{F\left(|m|-\nu',|m|+\nu'+1,|m|+1;\frac{1+\xi}{2}\right)}\Bigg|_{\xi=\cos\alpha}=0. \tag{18}$$

For given m, α, and V_0, we can determine ν from solving Eq. (18) numerically. In the limit of V_0 being very small, i.e., $\nu'\to\nu$, we can show that in order to satisfy Eq. (18) ν has to be a positive integer and equal to or greater than $|m|$. If the energy is very low compared with the potential barrier, that is, $\nu(\nu+1)<V_0-1/4$, then ν' is a complex number:

$$\nu'=-\frac{1}{2}\pm i\lambda, \tag{19a}$$

with

$$\lambda=\sqrt{V_0-1/4-\nu(\nu+1)}. \tag{19b}$$

Thus the function F in Eq. (15) for region $\alpha\le\theta\le\pi$ can be expressed in terms of conical function:[24,25]

$$F\left(|m|-\nu',|m|+\nu'+1,|m|+1;\cos^2\frac{\theta}{2}\right)=F\left(|m|+\frac{1}{2}-i\lambda,|m|+\frac{1}{2}+i\lambda,|m|+1;\cos^2\frac{\theta}{2}\right)$$
$$=1+\frac{\left[\left(|m|+\frac{1}{2}\right)^2+\lambda^2\right]}{1!\,(|m|+1)}\cos^2\frac{\theta}{2}$$
$$+\frac{\left[\left(|m|+\frac{1}{2}\right)^2+\lambda^2\right]\left[\left(|m|+\frac{3}{2}\right)^2+\lambda^2\right]}{2!\,(|m|+1)(|m|+2)}\cos^4\frac{\theta}{2}+\cdots. \tag{20}$$

Examining Eq. (18), we can find that if V_0 is very large, i.e., $V_0-1/4\gg\nu(\nu+1)$, the second term of Eq. (18) can be written as

$$\frac{\left(|m|+\frac{1}{2}\right)^2+\lambda^2}{(|m|+1)}\frac{\left[1+\frac{\left(|m|+\frac{3}{2}\right)^2+\lambda^2}{(|m|+2)}\cos^2\frac{\alpha}{2}+\frac{\left[\left(|m|+\frac{3}{2}\right)^2+\lambda^2\right]\left[\left(|m|+\frac{5}{2}\right)^2+\lambda^2\right]}{2!(|m|+2)(|m|+3)}\cos^4\frac{\alpha}{2}+\cdots\right]}{\left[1+\frac{\left(|m|+\frac{1}{2}\right)^2+\lambda^2}{(|m|+1)}\cos^2\frac{\alpha}{2}+\frac{\left[\left(|m|+\frac{1}{2}\right)^2+\lambda^2\right]\left[\left(|m|+\frac{3}{2}\right)^2+\lambda^2\right]}{2!(|m|+1)(|m|+2)}\cos^4\frac{\alpha}{2}+\cdots\right]}.$$

As λ approaches infinity, we have to set

$$F\left(|m|-\nu,|m|+\nu+1,|m|+1;\frac{1-\xi}{2}\right)_{\xi=\cos\alpha}=0. \tag{21}$$

We can easily notice that Eq. (21) is exactly the hard-wall case stated in Ref. 16.

III. RESULTS AND DISCUSSION

Rotational energy levels of a molecule can be obtained by using the relation $E^{\mathrm{rot}}_{\nu,m}=\nu(\nu+1)B$ where B is the rotational constant of the molecule. The values of rotational quantum number ν, for given azimuthal quantum number m, hindrance angle α, and dimensionless potential barrier height V_0, are determined by solving

Eq. (18) numerically. Unlike the free space rotor, the energies $E^{\rm rot}_{\nu,m}$ of the hindered rotor depend on m implicitly. In Figs. 2(a)–2(c), we present the calculated ten low-lying rotational energy levels as functions of the hindrance angle α for three different potential barrier heights, namely, $V_0 = 5$, 20, and 80. The hard-wall potential case, $V_0 = \infty$, is presented in Fig. 2(d) for the sake of comparison. In general, these figures exhibit clearly the influence of the rotational hindrance on the rotational energy. One can note that the oscillatory behavior, which occurs at small hindrance angle, disappears as the potential barrier height increases to infinity.

As $\alpha = 180°$, the rotor is free, the energy of the lth level reduces to $E^{\rm rot} = l\,(l+1)\,B$ with $(2l+1)$-fold degeneracy. When the hindrance angle decreases, the spatial confinement renders the increases of the rotational energy. Thus the degeneracy between the states with different values of $|m|$ is removed for both the hard-wall and soft-wall cases. In those cases, the rotational energies are no longer expressed in terms of the integral orbital quantum numbers l and, instead, they are expressed in terms of the new quantum numbers ν and m. The azimuthal quantum number m remains the same and relates to $E^{\rm rot}_{\nu,m}$ implicitly as mentioned previously, but the rotational quantum number ν is no longer an integer except for special cases. The variations with respect to the hindrance angle of the rotational energy levels of the hard-wall and soft-wall hindered rotors are rather different. In the case of the hard-wall hindered rotor, the rotational energy increases steadily as the confinement angle decreases. However, for the soft-wall hindered rotor, the rotational energy changes oscillatorily as the hindrance angle decreases. This behavior is primarily caused by the nonvanishing probability of the hindered rotor outside the potential well and can be realized, at first, in terms of the perturbation calculation as follows.

If the height of the finite-conical-well potential is small compared with the low-lying eigenenergies, its effect can be treated perturbatively. The energy of the hindered rotor can be approximated to the first order in V_0B as

$$E^{\rm rot}_{l,m} = l\,(l+1)\,B + V_0B\int_\alpha^\pi |Y_{l,m}\,(\theta,\phi)|^2\,2\pi\sin\theta d\theta$$
$$= l\,(l+1)\,B + V_0B - \frac{2l+1}{2}\frac{(l-m)!}{(l+m)!}V_0B$$
$$\times\int_0^\alpha |P_l^m\,(\cos\theta)|^2\sin\theta d\theta. \qquad (22)$$

Since Eq. (22) can be evaluated analytically for each Legendre polynomial P_l^m, the result of integration is just a polynomial of $\cos\alpha$ of degree $(2l+1)$. Thus the oscillations of the energy are governed by the orders (l,m) of the Legendre polynomials. Figure 3 presents the perturbative results of Eq. (22) for $V_0 = 5$. Comparing Fig. 3 with Fig. 2, the similarity between the energy levels calculated from two different schemes is very obvious.

From Fig. 2(a), we can see that for smaller barrier height, the energy levels can still be categorized in different groups in accordance with the quantum numbers l of the free rotor. But for larger barriers, the levels start to intersect with each other and those corresponding to larger l states of free rotor are no longer higher than those of the smaller l states. When the hindrance angle approaches zero, the rotational energy of the hard-wall hindered rotor diverges due to the infinite potential barrier. But on the other hand, because of the softness of the potential wall, the narrower conical well yields larger probability leaking outside the conical well. Therefore when the hindrance angle α approaches zero, the probability of finding the rotor outside the conical well is close to unity. The rotor becomes almost freelike again, but accompanied by an additional energy V_0B. Therefore the lth level of the rotor approaches $E^{\rm rot} = l\,(l+1)\,B + V_0B$ with $(2l+1)$-fold degeneracy.

In order to investigate further the variation of the hindered-rotor wave function, it is more helpful to plot the angular distributions of the hindered-rotor wave function:

$$D_{\nu,m}\,(\theta) = \left|\Psi^{\rm rot}_{\nu,m}\,(\theta,\phi)\right|^2 \qquad (23)$$

for different hindrance conditions. In Figs. 4–6, we show the angular distributions of three low-lying normalized

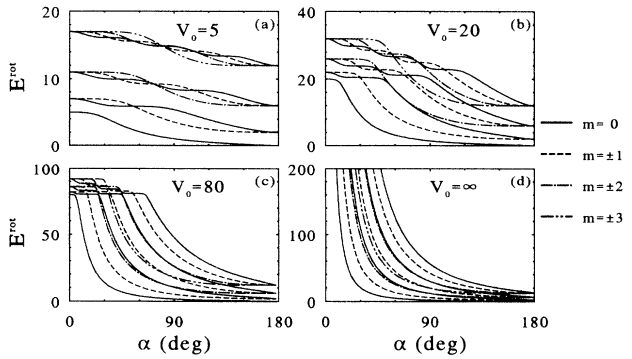

FIG. 2. The ten low-lying rotational levels of a hindered rotor as functions of the hindrance angle for potential barrier height (a) $V_0 = 5$, (b) $V_0 = 20$, (c) $V_0 = 80$, and (d) $V_0 = \infty$ (in units of $B = \hbar^2/2I$).

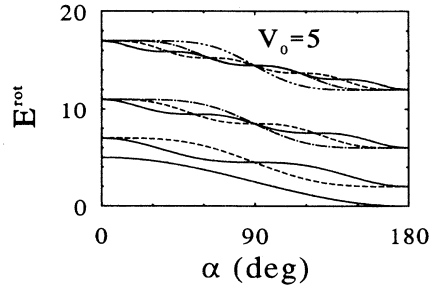

FIG. 3. The perturbative results of the ten low-lying rotational levels of a hindered rotor as functions of the hindrance angle for potential barrier height $V_0 = 5$ (in units of $B = \hbar^2/2I$).

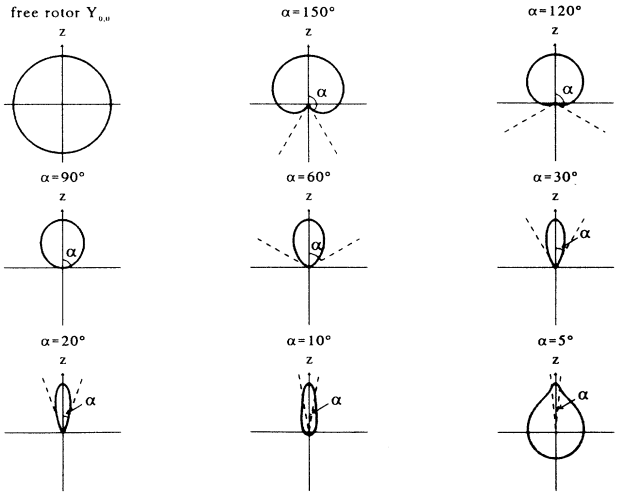

FIG. 4. Angular distributions of the finite-conical-well hindered-rotor wave function $\Psi^{\rm rot}_{\nu,0}$ for different hindrance angles and potential barrier height $V_0 = 20$. $\Psi^{\rm rot}_{\nu,0} = Y_{0,0}$ when the confinement potential is absent.

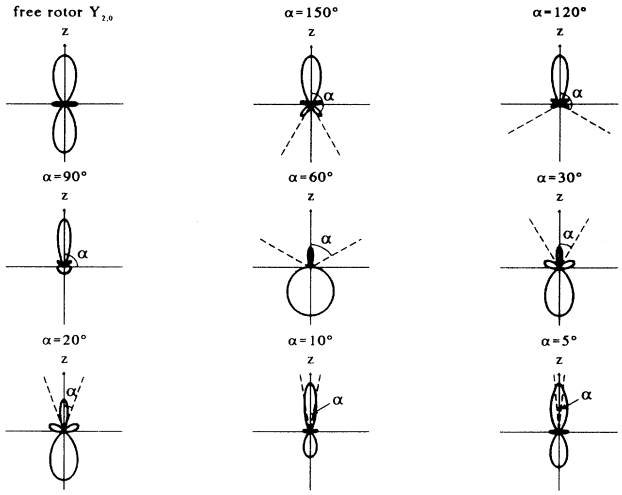

FIG. 6. Angular distributions of the finite-conical-well hindered-rotor wave function $\Psi^{\rm rot}_{\nu,0}$ for different hindrance angles and potential barrier height $V_0 = 20$. $\Psi^{\rm rot}_{\nu,0} = Y_{2,0}$ when the confinement potential is absent.

wave functions, $\Psi^{\rm rot}_{\nu,m}$, where ν is not necessarily an integer when $0° < \alpha < 180°$, $m = 0$, and $V_0 = 20$. In each figure, we present nine wave functions at different hindrance angles; they all started from free rotor states, $Y_{l,0}$, where $l = 0$, 1, and 2, when $\alpha = 180°$. From these figures, we notice the angular distributions of the rotor states change significantly when confined by the conical well. The azimuthal symmetry of the angular distribution is preserved, but the reflection symmetry with respect to the $\alpha = 90°$ plane is lost. For large hindrance angle, since the rotational energy is much less than the barrier height, the wave functions of the soft-wall and hard-wall hindered rotors are similar. As the hindrance angle decreases the wave functions are distorted due to the compression of the potential wall. When the potential barrier is infinite, the wave function must vanish at the boundary. Therefore, when α, the hindrance angle, changes from $\alpha = 180°$ to $\alpha = 90°$, the rotational state of the rotor changes from the free rotor state $Y_{l,m}$ to the half space rotor state $Y_{l',m}$, where

$$l' = 2l + 1 - |m|\,, \tag{24}$$

and l' and m satisfy the surface selection rule[26,27]

$$l' + m = \text{odd}. \tag{25}$$

For $\alpha \leq 90°$, the angular distribution of the hard-wall hindered-rotor wave function is compressed further while that of the soft-wall hindered rotor begins to leak outside the well, particularly those higher energy states. Figures 4–6 exhibit clearly that for small α, the behavior of the soft-wall hindered-rotor wave functions returns to that of the free space rotor again.

Examining the angular distributions in Figs. 5 and 6, we found that the confinement probability which is defined as the probability of the rotor appearing inside the conical well, i.e.,

$$P^{\rm in}_{\nu,m} = \int_0^{\alpha} \left|\Psi^{\rm rot}_{\nu,m}(\theta,\phi)\right|^2 2\pi \sin\theta d\theta, \tag{26}$$

for some smaller hindrance angles is larger than that for greater hindrance angles. To study the variation of $P^{\rm in}_{\nu,m}$ with the hindrance angle α, the confinement probability $P^{\rm in}_{\nu,m}$ as well as the energy levels $E^{\rm rot}_{\nu,m}$ for the three low-lying $m = 0$ rotational states are plotted in Fig. 7(a) for the case of $V_0 = 20$. For convenience, we denote

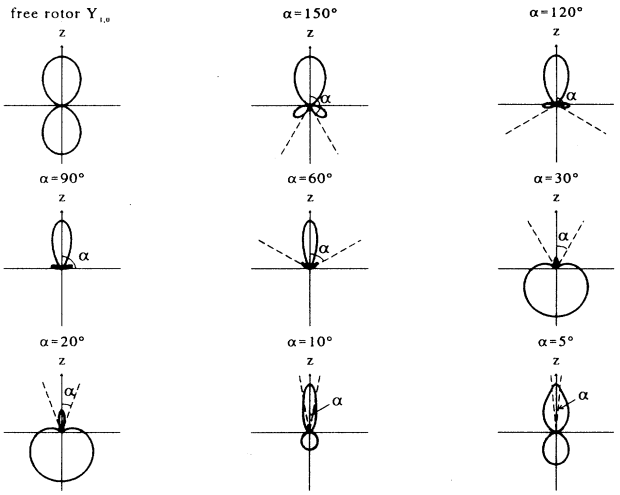

FIG. 5. Angular distributions of the finite-conical-well hindered-rotor wave function $\Psi^{\rm rot}_{\nu,0}$ for different hindrance angles and potential barrier height $V_0 = 20$. $\Psi^{\rm rot}_{\nu,0} = Y_{1,0}$ when the confinement potential is absent.

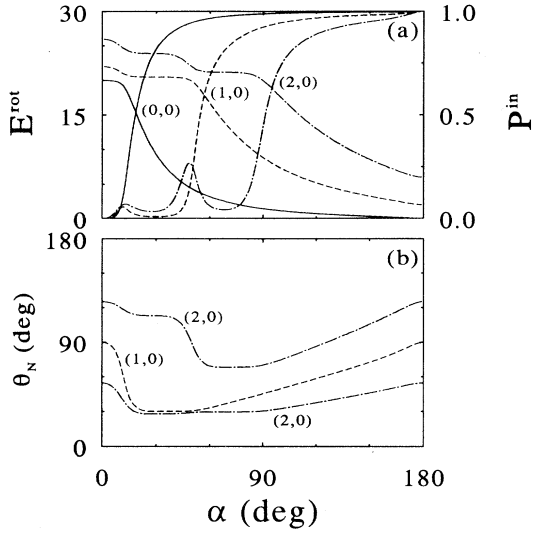

FIG. 7. (a) The energy level $E^{\rm rot}_{\nu,m}$ as well as the confinement probability $P^{\rm in}_{\nu,m}$ as functions of the hindrance angle α for the three low-lying $m = 0$ rotational states shown in Figs. 4–6. For convenience, these states are denoted by (0,0), (1,0), and (2,0), respectively. (b) The node positions θ_N of wave functions of states (1,0) and (2,0) as functions of the hindrance angle α.

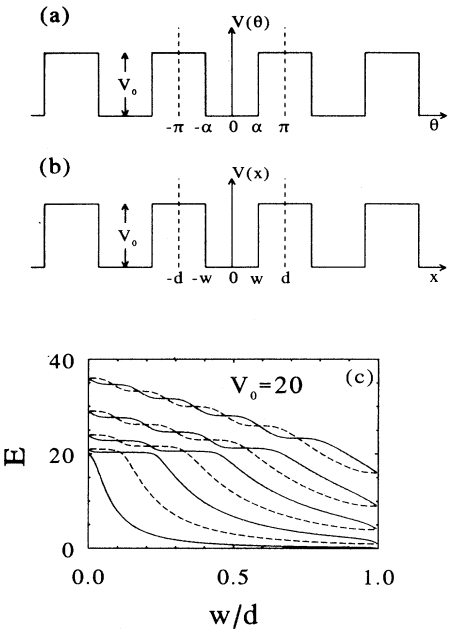

FIG. 8. (a) The finite-conical-well potential of hindered rotor in polar angle θ. (b) The Kronig-Penney type potential in Cartesian coordinate x. (c) The low-lying energy levels (solid curves for the even parity states and dashed curves for the odd parity states) of a particle moving in the Kronig-Penney potential shown in (b) as functions of w/d for $V_0 = 20$ (in units of $B' = \pi^2\hbar^2/2md^2$).

these states by (0,0), (1,0), and (2,0), respectively. One can find from Fig. 7(a) that $P^{\rm in}_{\nu,m}$ displays the oscillatory behavior as $E^{\rm rot}_{\nu,m}$ does. Furthermore, the numbers of oscillations of $P^{\rm in}_{\nu,m}$ and $E^{\rm hin}_{\nu,m}$ are the same for each state.

The above mentioned oscillatory behaviors in $P^{\rm in}_{\nu,m}$ and $E^{\rm rot}_{\nu,m}$ do not appear in the one-dimensional finite single square well. In the finite single square well case the energy decreases and the confinement probability increases steadily as the well width increases. The essential reason for this particular feature is intimately related to the rotational symmetry of the conical well problem, whereas in the finite single square well case, the wave functions of a particle outside the square well decay exponentially as $|x|$ approaches infinity. However, the hindered-rotor wave functions of the finite conical well do not have to vanish anywhere. Instead, they have to be rotationally invariant, i.e., $\Psi^{\rm rot}_{\nu,m}(\theta + 2n\pi, \phi) = \Psi^{\rm rot}_{\nu,m}(\theta, \phi)$. Therefore the present eigenvalue problem involves a periodic potential of polar angle θ, and is equivalent to the case of the one-dimensional Kronig-Penney type potential[21] in Cartesian coordinate x. The analog of the periodic potential involved in the finite-conical-well hindered rotor and Kronig-Penney type problem can be found in Figs. 8(a) and 8(b). The requirement of the rotational invariant of the hindered-rotor wave functions for a finite conical well $\Psi^{\rm rot}_{\nu,m}(\theta + 2n\pi, \phi) = \Psi^{\rm rot}_{\nu,m}(\theta, \phi)$ as shown in Fig. 8(a) is equivalent to the requirement of the translational invariant of the particle wave functions $\Psi(x + 2nd) = \Psi(x)$ for a Kronig-Penney potential well as shown in Fig. 8(b). The solutions of the Kronig-Penney type potential can be expressed as

$$\Psi_{\rm even}(x) = \begin{cases} A_{\rm II,even}\cosh[\kappa(x+d)] & \text{for } -d \le x < -w \\ A_{\rm I,even}\cos(kx) & \text{for } -w \le x < w \\ A_{\rm II,even}\cosh[\kappa(x-d)] & \text{for } w \le x < d \end{cases} \tag{27a}$$

for even parity states and

$$\Psi_{\rm odd}(x) = \begin{cases} A_{\rm II,odd}\sinh[\kappa(x+d)] & \text{for } -d \le x < -w \\ A_{\rm I,odd}\sin(kx) & \text{for } -w \le x < w \\ A_{\rm II,odd}\sinh[\kappa(x-d)] & \text{for } w \le x < d \end{cases} \tag{27b}$$

for odd parity states, where

$$k = \left(\frac{2mE}{\hbar^2}\right)^{1/2}, \tag{27c}$$

$$\kappa = \left(\frac{2m(V_0 - E)}{\hbar^2}\right)^{1/2}, \tag{27d}$$

and A is normalization constant. The eigenvalues E can be determined by solving

$$k\sin(kw)\cosh[\kappa(d-w)]$$

$$-\kappa\cos(kw)\sinh[\kappa(d-w)] = 0 \tag{27e}$$

for even parity states and

$$\kappa \sin(kw)\cosh[\kappa(d-w)] + k\cos(kw)\sinh[\kappa(d-w)] = 0 \quad (27f)$$

for odd parity states. The above equations are still valid for the case of $E > V_0$ providing that κ is replaced by $i\kappa'$ with

$$\kappa' = \left(\frac{2m(E-V_0)}{\hbar^2}\right)^{1/2}. \quad (27g)$$

The low-lying energy levels of a particle moving in the Kronig-Penney type potential shown in Fig. 8(b) are presented in Fig. 8(c) as functions of w/d for $V_0 = 20$, where $2w$ is the well width. The energies are expressed in terms of $B' = \pi^2\hbar^2/2md^2$. The similarities between Fig. 8(c) and Fig. 2 are obvious. As $w/d = 1$, i.e., the potential barriers are absent, the particle is free. However, due to the periodic boundary condition $\Psi(x+2d) = \Psi(x)$, the energy levels are discrete. The energy of the nth level is $E = n^2B'$, where $n = 0, 1, 2, \ldots$. Excepting the ground state, the energy levels are twofold degenerate with even and odd parity. As w/d approaches zero, the particle becomes almost freelike again, but accompanied by an additional energy V_0B'. Therefore the energy of the nth level approaches $E = n^2B' + V_0B'$. In the region of $0 < w/d < 1$, the levels are oscillatory for energies above the square barrier. This oscillatory behavior is very similar to that of the hindered rotor as shown in Fig. 2.

From the comparison between the Kronig-Penney type potential and the finite conical well of the hindered-rotor problem, the physical origin of the oscillatory behavior of $E^{\rm rot}$ as functions of the confinement angle α as shown in Fig. 2 can be easily understood. The oscillatory behavior of E as functions of w/d in the Kronig-Penney type potential is ascribed to the phenomenon of the resonance transmission. In our case, for larger hindrance angle α, the rotational energy is less than the barrier height and the state is bounded. As the hindrance angle decreases, the rotational energy of the rotor increases due to the uncertainty relation. When α decreases further, the energies of higher excited states increase further until they are larger than the barrier height. In this situation, the higher excited states become unbounded, however, due to the periodic boundary condition, their energies are still discrete. Contrary to the level energy, the probabilities $P^{\rm in}$ for these states of the rotor appearing in the conical well decrease as α decreases. When α equals some particular value θ_N so that the potential wall is located on the node position of the wave function [i.e., $\Theta(\theta_N) = 0$], the wave function vanishes at this particular angle $\alpha = \theta_N$. Therefore the waves (reflected and incident) inside the well interfere destructively with each other, and the resonance transmission occurs. Thus $P^{\rm in}$ in the case of $\alpha = \theta_N$ is minimum as shown in Fig. 7(a). As α decreases further, the node of the wave function does not coincide with the potential wall again. The resonance transmission disappears, thus $P^{\rm in}$ increases until the location of the potential wall approaches the next node. In Fig. 7(b), the node positions θ_N of wave functions of states (1,0) and (2,0) are plotted as functions of the hindrance angle α. From Fig. 7, one can note that $P^{\rm in}$ approaches minimum at $\theta_N = \alpha \sim 30°$ for state (1,0) and at $\theta_N = \alpha \sim 30°$ and $\sim 70°$ for state (2,0). The number of oscillations of $P^{\rm in}_{\nu,m}$ is equal to the number of nodes of $\Psi^{\rm in}_{\nu,m}$ between $0 < \theta < 180°$. The rotational energy $E^{\rm rot}$ oscillates as $P^{\rm in}$ oscillates. When $P^{\rm in}$ is around its minimum, $E^{\rm rot}$ is less sensitive to the change of α, thus $E^{\rm rot}$ increases very gently as α decreases. On the other hand, when $P^{\rm in}$ is around its maximum, $E^{\rm rot}$ is more sensitive to the change of α, thus $E^{\rm rot}$ increases rapidly as α decreases. This relation between $E^{\rm rot}$ and $P^{\rm in}$ can be noted from Fig. 7(a). Thus we may conclude that the particular oscillatory behavior of $P^{\rm in}$ and $E^{\rm rot}$ can be regarded as the manifestation of the rotational invariance of the hindered-rotor problem.

The eigenvalues and eigenfunctions of the soft-wall hindered rotor were utilized to calculate the rotational-state distributions of molecules desorbed from a solid surface. We applied the sudden unhindrance approximation used in the works of Gadzuk and co-workers.[16–18] This approximation is based on the argument that if the desorption is induced by a fast process, the hindering potential is suddenly switched off and pure hindered-to-free rotational transition with no wave function alteration takes place. The free rotation is described by a set of spherical harmonics: $\{Y_{l,m}(\theta,\phi)\}$, thus the rotational-state distribution is given by a sum of rotational Franck-Condon factors between $Y_{l,m'}$ and $\Psi^{\rm rot}_{v,m}$ weighted by appropriate thermal factors, that is,

$$P(l) = \frac{1}{Z_{\rm hin}} \sum_{v,m,m'} \exp[-B\nu(\nu+1)/kT] \times |\langle Y_{l,m'} \mid \Psi^{\rm rot}_{v,m}\rangle|^2, \quad (28)$$

where T is the ambient temperature, k is the Boltzmann constant, and $Z_{\rm hin}$ is the partition function of the hindered rotor.

In Fig. 9, the calculated rotational-state distributions based on Eq. (28) with various potential barrier heights and $B/kT = 1$ are shown. From these figures, we can see that the rotational-state distributions are significantly influenced by the potential barrier height and hindrance angle. At low enough temperature, the hindered rotor is primarily located at low-lying states. Thus the population of the final high-l states depends mainly on their overlaps with the low-lying ν states. However, for small potential barrier height and small confinement angle, the rotational-state distribution behaves very similarly to that of the free rotor. For example, when $V_0 = 5$, all of the curves are alike [Fig. 9(a)], but as V_0 increases to 20, only the $\alpha = 10°$ curve is similar to that of the free rotor [Fig. 9(b)]. This can be easily understood by investigating the wave functions of the finite-well rotors (Figs. 4–6). We can see that the hindrance angle as well as the finite potential act together to confine the rotor. Unlike the infinite potential barrier, the probability of the rotor confined within the finite conical well may sometimes be smaller than that outside the well. This can be understood as the interplay between the poten-

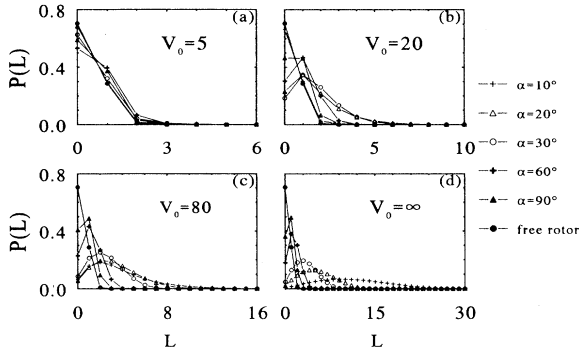

FIG. 9. Rotational-state distributions of a suddenly unhindered rotor as function of the free-rotor rotational quantum number for different hindrance angles with $B/kT = 1$ and potential barrier heights (a) $V_0 = 5$, (b) $V_0 = 20$, (c) $V_0 = 80$, and (d) $V_0 = \infty$. The $\alpha = 10°$ curve in (a) is coincident with that of the free rotor in this case.

tial energy caused by the potential barrier and the uncertainty principle which primarily relates to the kinetic energy due to confinement. That is, when we gradually increase the height of the conical wall and reduce the hindrance angle, energies of the low-lying ν states start to increase and the overlaps of the low-lying ν states with the high-l states become more prominent. This explains why the final-state distributions turn wider or "hotter" when the conical wells become narrower. In addition, we also found that the distribution is independent of the ambient temperature.[16–18] From Figs. 9(b) and 9(c), we witness the progression of such change as we vary the potential barrier height and hindrance angle. Therefore, when the potential barrier height is sufficiently large or the conical well is not too narrow, the rotational-state distributions display characteristics similar to those of the hard-wall rotors [Figs. 9(c) and 9(d)].

IV. CONCLUSIONS

We have studied the hindered rotational motion of a molecule adsorbed vertically by a solid surface. Here, we modeled the surface potential by a finite conical well which confines the rotational motion of the rotor so that the rotor is free inside the well but hindered outside. Since the Hamiltonian of the hindered rotor is invariant under rotation, i.e., $\theta \rightarrow \theta + 2n\pi$, we cannot prescribe an exponentially decaying function in the finite barrier region as in the situation of its Cartesian analog. After proper transformation, we found that there are two singularities, namely, $\theta = 0°$ and 180°, respectively. Due to the presence of the finite potential barrier, each of them is located at separate regions. Wave functions in both regions can be expressed in terms of the hypergeometric functions. The quantization condition for the eigenvalues can be obtained by matching the derivatives of different solutions in each region at the boundary. For given values of the hindrance angle and potential barrier height, the matching equations can be solved numerically and the entire rotational energy spectra and eigenfunctions are thus obtained. Our results showed that the rotational energy levels increase as the hindrance angle decreases. The main difference between the rotational energy levels of the infinite- and finite-conical-well model is that, in the case of the infinite conical well, the levels increase monotonically as the hindrance angle decreases. But for the finite-conical-well model, the levels increase oscillatorily as the hindrance angle decreases and eventually approach the rotational levels of the free space rotor with a constant background potential energy, which is the height of the potential barrier. The angular distributions of the soft-wall hindered rotor were plotted for the low-lying three $m = 0$ rotational states. These figures clearly display that the shapes of the angular wave functions of the hindered rotor are significantly influenced by the compression of the hindrance wall. We also presented the confinement probabilities of the hindered rotor; similar oscillatory behaviors were found. The oscillatory behavior of energy levels and confinement probabilities are due to the occurrence of resonance transmission of wave functions at some hindrance angle, and can be regarded as the manifestation of the rotational invariance of the hindered-rotor problem.

By employing the sudden unhindrance approximation, the solutions of the hindered rotor were used to calculate the rotational-state distribution of molecules desorbed from a solid surface. In the calculated results, we showed that, similar to the hard-wall case, for sufficiently high potential barrier and low temperature, the final-state distributions are hotter when the conical well is narrower, independent of the ambient temperature. On the other hand, for low enough potential barrier and narrow conical well, due to the fact that the hindered rotor is almost freelike, the final-state distributions are not different from those of Boltzmann type.

ACKNOWLEDGMENT

This work was supported by the National Science Council, Taiwan, Republic of China.

* Author to whom all correspondence should be addressed.
† On leave from Department of Physics, University of Nebraska at Omaha, Omaha, Nebraska 68182.

[1] F. Frenkel, J. Hager, W. Krieger, H. Walther, C. T. Campbell, G. Ertl, H. Kuipers, and J. Segner, Phys. Rev. Lett. **46**, 152 (1981).
[2] A. W. Kleyn, A. C. Luntz, and D. J. Auerbach, Phys. Rev. Lett. **47**, 1169 (1981).
[3] D. Weide, P. Audresen, and H.-J. Freund, Chem. Phys. Lett. **136**, 106 (1987).

[4] G. O. Sitz, A. C. Kummel, and R. N. Zare, J. Chem. Phys. **89**, 2558 (1988).
[5] B. H. Choi, Z. B. Guvenc, and N. L. Liu, Phys. Rev. B **42**, 3887 (1990).
[6] R. R. Cavanagh and D. S. King, Phys. Rev. Lett. **47**, 1829 (1981).
[7] D. S. King, D. A. Mantell, and R. R. Cavanagh, J. Chem. Phys. **82**, 1046 (1985).
[8] D. A. Mantell, R. R. Cavanagh, and D. S. King, J. Chem. Phys. **84**, 5131 (1986).
[9] A. R. Burns, Phys. Rev. Lett. **55**, 525 (1985).
[10] S. A. Buntin, L. J. Richter, R. R. Cavanagh, and D. S. Kink, Phys. Rev. Lett. **61**, 1321 (1988).
[11] F. Budde, A. V. Hamza, P. M. Ferm, G. Ertl, D. Weide, P. Andresen, and H.-J. Freund, Phys. Rev. Lett. **60**, 1518 (1988).
[12] E. Hasselbrink, S. Jakubith, S. Nettesheim, M. Wolf, A. Cassuto, and G. Ertl, J. Chem. Phys. **92**, 3154 (1990).
[13] J. Xu, A. Barnes, R. Albridge, C. Ewig, and N. Tolk, Phys. Rev. B **48**, 8222 (1993).
[14] P. D. Pacey, J. Chem. Phys. **77**, 3540 (1982).
[15] V. M. Allen and P. D. Pacey, Surf. Sci. **177**, 36 (1986).
[16] J. W. Gadzuk, Uzi Landman, E. J. Kuster, C. L. Cleveland, and R. N. Barnett, Phys. Rev. Lett. **49**, 426 (1982).
[17] Uzi Landman, Isr. J. Chem. **22**, 339 (1982).
[18] J. W. Gadzuk, Uzi Landman, E. J. Kuster, C. L. Cleveland, and R. N. Barnett, J. Electron. Spectrosc. Relat. Phenom. **30**, 103 (1983).
[19] Uzi Landman, G. G. Kleiman, C. L. Cleveland, E. Kuster, R. N. Barnett, and J. W. Gadzuk, Phys. Rev. B **29**, 4313 (1984).
[20] S. Krempl, Surf. Sci. **259**, 183 (1991).
[21] R. de L. Kronig and W. G. Penney, Proc. R. Soc. London Ser. A **130**, 499 (1931).
[22] M. D. Alvey and J. T. Yates, Jr., J. Chem. Phys. **87**, 7221 (1987).
[23] Y. T. Shih, D. S. Chuu, and W. N. Mei (unpublished).
[24] *Handbook of Mathematical Functions*, edited by Milton Abramowitz and Irene A. Stegun (Dover, New York, 1970).
[25] *Higher Transcendental Functions*, edited by A. Erdelyi (McGraw-Hill, New York, 1953), Vol. I.
[26] J. D. Levine, Phys. Rev. **140**, A586 (1965).
[27] J. W. Gadzuk, Phys. Rev. **154**, 662 (1967).

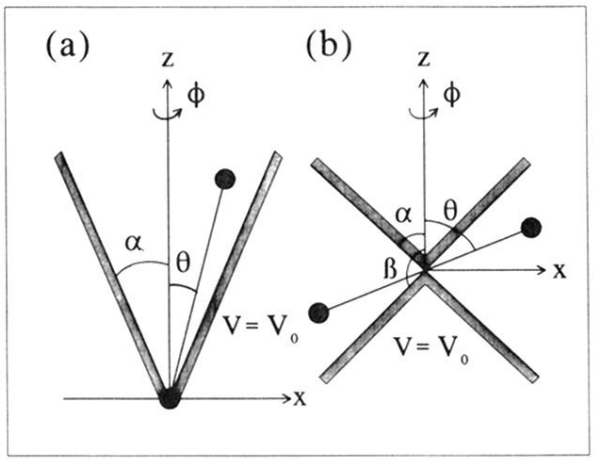

FIG. 1. (a) Schematic of the finite-conical-well hindering potential for vertical adsorption configuration. (b) Schematic of the finite-conical-well hindering potential for horizontal adsorption configuration.